tvst

Article

Generation of a Retina Reporter hiPSC Line to Label Progenitor, Ganglion, and Photoreceptor Cell Types

Phuong T. Lam, Christian Gutierrez, Katia Del Rio-Tsonis, and Michael L. Robinson

Department of Biology and Center for Visual Sciences, Miami University, Oxford, OH, USA

Purpose: Early in mammalian eye development, *VSX2*, *BRN3b*, and *RCVRN* expression marks neural retinal progenitors (NRPs), retinal ganglion cells (RGCs), and photoreceptors (PRs), respectively. The ability to create retinal organoids from human induced pluripotent stem cells (hiPSC) holds great potential for modeling both human retinal development and retinal disease. However, no methods allowing the simultaneous, real-time monitoring of multiple specific retinal cell types during development currently exist.

Methods: CRISPR/Cas9-mediated homology-directed repair (HDR) in hiPSCs facilitated the replacement of the *VSX2* (Progenitor), *BRN3b* (Ganglion), and *RCVRN* (Photoreceptor) stop codons with sequences encoding a viral P2A peptide fused to Cerulean, green fluorescent protein, and mCherry reporter genes, respectively, to generate a triple transgenic reporter hiPSC line called PGP1. This was accomplished by co-electroporating HDR templates and sgRNA/Cas9 vectors into hiPSCs followed by antibiotic selection. Functional validation of the PGP1 hiPSC line included the ability to generate retinal organoids, with all major retinal cell types, displaying the expression of the three fluorescent reporters consistent with the onset of target gene expression. Disaggregated organoids were also analyzed by fluorescence-activated cell sorting and fluorescent populations were tested for the expression of the targeted gene.

Results: Retinal organoids formed from the PGP1 line expressed appropriate fluorescent proteins consistent with the differentiation of NRPs, RGCs, and PRs. Organoids produced from the PGP1 line expressed transcripts consistent with the development of all major retinal cell types.

Conclusions and Translational Relevance: The PGP1 line offers a powerful new tool to study retinal development, retinal reprogramming, and therapeutic drug screening.

Introduction

Stem cells provide multiple avenues to address irreversible vision loss associated with retinal cell death caused by trauma or by disease. Common diseases, including age-related macular degeneration (AMD) and glaucoma, lead to irreversible blindness, costing billions of dollars in social welfare and lost productivity.[1,2] Recent advancements in three-dimensional culture have led to the development of retinal organoids consisting of all major retinal cell types from human induced pluripotent stem cells (hiPSCs).[3] These hiPSC-derived organoids can model normal neural retinal (NR) development and progression of retinal disease. Additionally, organoids provide a platform to screen drugs for the treatment of retinal degeneration.[3,4] Finally, hiPSCs can potentially make unlimited numbers of specific retinal neurons for transplantation therapies.

The rapidly expanding use of hiPSCs to model human retina justifies the need for tools to monitor the appearance of specific cell types without interrupting normal development. For this purpose, CRISPR/Cas9 gene editing facilitates the insertion of cell type–specific reporters into hiPSCs. Although several hiPSCs with single reporter knock-ins exist,[5–7] these lines only detect terminally differentiated retinal cell types, which

translational vision science & technology

limits the ability to study progression of retinal development in real time. Having multiple cell type reporters inserted into the same genome will permit specific cell sorting and allow for the optimization of protocols that enrich for the development of particular retinal cell types. For example, one might need a large number of photoreceptors (PRs) or retinal ganglion cells (RGCs) to screen for drugs to treat AMD or glaucoma, respectively.[8,9]

To address these limitations, we used CRISPR/Cas9 to insert reporter genes encoding fluorescent proteins into the *VSX2*, *BRN3b*, and *RCVRN* loci in hiPSCs to make it possible to monitor the differentiation of neural retinal progenitors (NRPs), RGCs, and PR cells, respectively. *VSX2* encodes a transcription factor that marks NRPs.[10] In the mature NR, only postmitotic bipolar cells express *VSX2*.[11–13] RGCs represent the first mature NR cell type to develop, and most RGCs express the BRN3b transcription factor.[12] PRs (rods and cones) express RCVRN, a protein important in the recovery phase of visual excitation.[14] The cell type–specific expression pattern of these genes made them appropriate targets for fluorescent protein expression. Given their importance in retinal development and/or function, we sought to retain the function of both alleles of all three (*VSX2*, *BRN3b*, and *RCVRN*) genes in engineered hiPSCs by using viral P2A peptides to create fusion genes between the target and the fluorescent reporter that would self-cleave upon translation.[15] Therefore, we inserted a P2A:Cerulean reporter into the *VSX2* locus, a P2A:eGFP reporter into the *BRN3b* locus, and a P2A:mCherry reporter into the *RCVRN* locus by replacing the stop codon of the endogenous gene with the P2A:reporter.

Methods

Specific Single-Guide RNA Vector (sgRNA) Design

CRISPR specific guide RNAs (Supplementary Table S1) were individually cloned into a PX458 vector that includes the *Streptococcus pyogenes* Cas9 (#48138; Addgene, Watertown, MA) as described.[16] To determine Cas9-sgRNA cutting efficiency, we transfected each vector into human embryonic kidney 293 (HEK293) cells. After 48 hours, HEK293 DNA was extracted and amplified by Q5 High-Fidelity PCR (M0494S; NEB, Ipswich, MA) using primers encompassing the sgRNA recognition site. The polymerase chain reaction (PCR) products were digested with T7 Endonuclease I (M0302S; NEB) as described.[17]

Successful Cas9 cleavage by sgRNAs resulted in two distinct bands in the T7E1 assay.

Homology-Directed Repair (HDR) Template Generation

To generate the HDR templates, the left and right homology arms (HAs) of each locus were amplified from the wild-type (WT) hiPSC genomic DNA (see Supplementary Table S2). The amplified HAs of *VSX2*, *BRN3b*, and *RCVRN* genes were inserted into the previously assembled vectors FRT.TK.Puro.FRT.pL451, LoxP.TK.Blast.LoxP.pL452, and FRT.TK.Neo.FRT.pL451 via Gibson Assembly (E2611L[18]; NEB), respectively (vector sequences available upon request). These insertions were confirmed by DNA sequencing. The Cerulean fluorescent reporter gene was derived from pCS-membrane-CeruleanFP, a gift from Sean Megason (Addgene plasmid 53749).[19] The GAP43-eGFP reporter gene was derived from pCAG-mGFP, a gift from Connie Cepko (Addgene plasmid 14757).[20] The mCherry reporter gene was derived from pEF6V5:eGFP-CAAX-2A-mCherry, a gift from Steven Leach (Addgene plasmid 26901).[21]

Insertion of Fluorescent Reporter Genes into Selected Loci

To generate the RCVRN/mCherry hiPSCs, we transfected 2.5 µg of the HDR template and 2.5 µg of the sgRNA vector into WT hiPSCs (hiPSC6.2[22,23] from Life Technologies, Carlsbad, CA; A18945) using a 4D-Nucleofector-X-Unit and the P3-Primary-kit (V4XP-3012; Amaxa, Cologne, Germany) based on the manufacturer's protocol. After transfection, cells were cultured with Essential 8 media plus 10 µM ROCK inhibitor (SCM075; Sigma, St. Louis, MO) overnight, with subsequent daily media changes without ROCK inhibitor. Antibiotic selection began after 48 hours with 100 µg/mL and slowly increased to 250 µg/mL of G418 (30234CR; Corning, Corning, NY) over the course of 1 week. DNA from resistant clones was extracted (D3025; Zymo Research, Irvine, CA) and screened for reporter integration by PCR and validated by DNA sequencing. A single RCVRN/mCherry hiPSC line was transfected with 1.25 µg each of the BRN3b:eGFP HDR template, the sgRNA vector to the *BRN3b* locus, the VSX2:Cerulean HDR template, and the sgRNA vector to the *VSX2* locus using nucleofection as described above. Double antibiotic selection was performed using 100 µg/mL each of blasticidin (ant-bl-05; InvivoGen, San Diego, CA) and puromycin (ant-pr-1; InvivoGen) and slowly increased

up to 250 μg/mL of each antibiotic over the course of 1 week to select for blasticidin/puromycin resistant colonies. All resistant clones were screened for reporter integration by PCR (see Supplementary Table S2) and validated by DNA sequencing.

Off-Target Screening

The PGP1 line was screened by selecting five high-scoring off-target sites for each sgRNA provided by Benchling (San Francisco, CA).[24] Each potential sgRNA off-target site (Supplementary Table S3) was screened by High-Fidelity PCR (Q5 NEB, M0491L) with primers listed in Supplementary Table S4, and PCR products were sequenced by Eurofins Genomics (Louisville, KY). Each result was independently repeated five times.

Three-Dimensional Retinal Organoid Generation from the PGP1 Triple Targeted Line

PGP1 retinal organoids were created using the Zhong et al.[25] protocol with modifications. Briefly, hiPSCs were incubated in 0.5 mM EDTA/DPBS (15575020; ThermoFisher, Waltham, MA) for 5 minutes at 37°C, prior to dissociation and culturing in mTeSR1 (85850; Stemcell Technologies, Vancouver, Canada) with 10 μM ROCK inhibitor (SCM075; Sigma) to form aggregates. The aggregates were gradually transitioned into neural induction medium (NIM)[25] from day (D) 1 to D3 of differentiation, then cultured in NIM from D3 to D6. On D7, the aggregates were seeded on Matrigel (hESC qualified, Corning 354277)–coated dishes in NIM at an approximate density of 20 aggregates per cm^2 and switched to Dulbecco's modified Eagle's medium (DMEM)/F12 (11320082; ThermoFisher) (3:1) supplemented with 2% Gem21 NeuroPlex (without vitamin A, 400-161; Gembio, Sacramento, CA), 1× NEAA (Non-Essential Amino Acids), and 1% antibiotic-antimycotic (15240062; ThermoFisher) on D16, with medium changes every third day. On D28 of differentiation, cells were detached, transferred to Petri dishes, and cultured in suspension in DMEM/F12 (3:1) supplemented with 2% Gem21 NeuroPlex, 1× NEAA (11140050; ThermoFisher), and 1% antibiotic-antimycotic (15240096; ThermoFisher). Within 3 to 5 days, cells began forming three-dimensional retinal organoids. The organoids were then mechanically separated from the rest of the cells using sharpened tungsten needles under a dissecting microscope. From that point on, the medium was changed twice a week.

To culture the retinal organoids long term, the medium was supplemented with 10% fetal bovine serum (FBS) (26140079; ThermoFisher), and 2 mM GlutaMax (35050061; ThermoFisher) beginning on D42.

Reverse Transcription–PCR (RT-qPCR) Analysis of Retinal Organoids

RNA isolation of retinal organoids was done using Quick RNA miniprep (R1057; Zymo Research). Reverse transcription was performed using the ImProm-II Reverse Transcription System (A3800; Promega, Madison, WI). RT-qPCR was performed with GoTaq qPCR Master Mix (A6001; Promega) using a CFX Connect Bio-Rad qPCR System. Forty cycles were run at 95°C denaturation for 40 seconds, 60°C annealing for 40 seconds, and 72°C extension for 60 seconds, using primers listed in Supplementary Table S5. The expression levels of genes were normalized to GAPDH messenger RNA (mRNA) levels and analyzed using the delta-delta Ct method with significant differences revealed by a two-tailed Student *t* test. Error bars in each figure represents the standard error of the mean (SE) of three individual experiments.

Immunofluorescence of the Retinal Organoids

Organoids were fixed with 4% paraformaldehyde (15710; ThermoFisher) for 20 minutes at room temperature, incubated in 30% sucrose overnight at 4°C, and embedded in OCT (95057-838; VWR, Radnor, PA). Organoids were cryosectioned at 15 μm and immunofluorescence was performed using antibodies listed in Supplementary Table S6 with images acquired using a Nikon (Melville, NY) Eclipse 80i microscope or Zeiss (Jena, Germany) LSM 710 Laser Scanning Confocal System. Residual fluorescence from the fluorescent proteins failed to survive our fixation and embedding protocol and therefore did not interfere with immunofluorescence studies (Supplementary Figs. S1, S2).

Fluorescence-Activated Cell Sorting (FACS) Analysis of the Retinal Organoids

Thirty organoids each from D55 and D135 were enzymatically dissociated in Accutase (AT104; Innovative Cell Technologies, San Diego, CA), and filtered through a 40-μm strainer (22-363-547; ThermoFisher) to get single cells and resuspended in ice-cold 5% FBS/1× HBSS (Hanks Balanced Salt Solution) (14-025-092; ThermoFisher) at a concentration of

10 million cells/mL. These cells were filtered again through a second strainer (08-771-23; ThermoFisher) prior to sorting. At D55, single cells were sorted for Cerulean positive (Cerulean⁺) and negative (Cerulean⁻) populations, as well as the eGFP-positive (eGFP⁺) and eGFP-negative (eGFP⁻) populations using a FACSMelody Cell Sorter (BD Biosciences, Franklin Lakes, NJ). For the D135, single cells were sorted for mCherry-positive (mCherry⁺) and mCherry-negative (mCherry⁻) populations. The sorted populations were used to measure mRNA transcripts for Cerulean, *VSX2*, eGFP, *BRN3b*, mCherry, *RCVRN*, and *GAPDH* via RT-qPCR (Supplementary Table S7). Gates for sorting disaggregated retinal organoids were established in a previous experiment using HEK293 cells transiently transfected with an expression plasmid for Cerulean, eGFP, or mCherry. FACS was conducted 48 hours after transfection to determine the appropriate gates for each fluorescent protein (Supplementary Fig. S3). In addition, organoids produced from WT hiPSCs were used to established negative gates.

Results

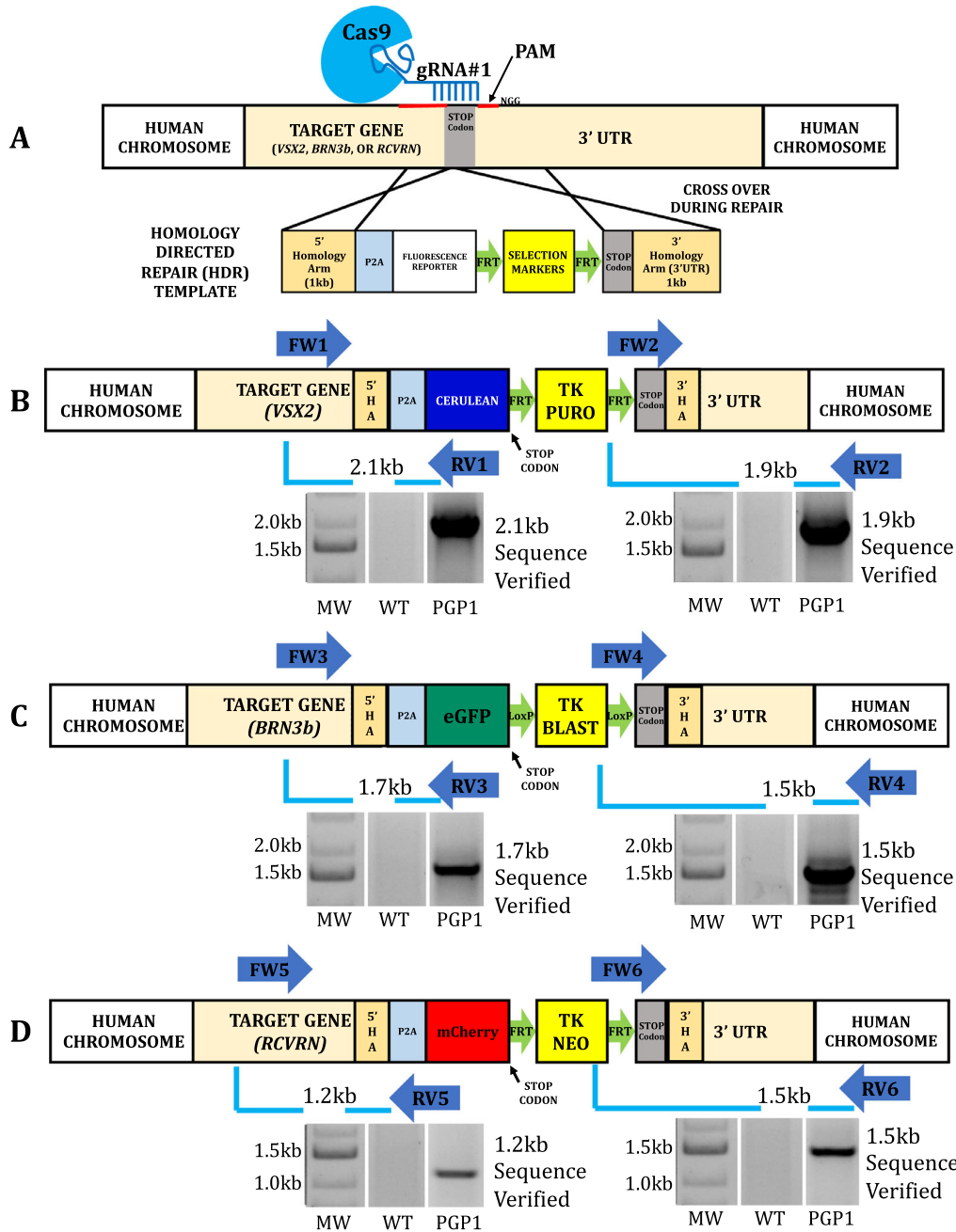### Creation of the Neural Retinal Progenitor/Retinal Ganglion/Photoreceptor (PGP1) Reporter

CRISPR/Cas9-mediated HDR (Fig. 1A) facilitated the replacement of the endogenous stop codons of the *VSX2*, *BRN3b*, and *RCVRN* genes with a P2A peptide fused to a fluorescent reporter gene. Briefly, hiPSCs were nucleofected with a *S pyogenes* Cas9 expression vector (containing appropriate sgRNAs) and HDR templates targeting each locus. Antibiotic resistant clones were tested by DNA sequence analysis of two PCR amplicons (Supplementary Table S8) encompassing the 5′ and 3′ ends of the targeted modification with at least one PCR primer outside of the HA (Figs. 1B–D). The *RCVRN* locus was first targeted independently, resulting in 48 G418 resistant hiPSC clones, with three (6.25%) clones verified as correctly targeted by DNA sequencing of PCR amplicons (Fig. 1D). Simultaneous targeting of the *VSX2* and *BRN3b* loci from one of these clones yielded 144 clones resistant for both puromycin and blasticidin. PCR genotyping followed by DNA sequencing identified four (2.8%) of these triple antibiotic-resistant clones (56, 101, 108, and 122) as correctly targeted at all three targeted loci. We randomly designated one (122) of these triple targeted hiPSC clones (PGP1) for further molecular and functional analyses.

A three-primer PCR strategy, using the forward primer outside 5′HA, with two different reverse primers made it possible to determine if the PGP1 line was heterozygous or homozygous at each locus. All three loci yielded PCR amplicons with expected band sizes for WT and targeted alleles (Fig. 2). Sequence analysis from the WT PGP1 alleles failed to reveal indel mutations at the sgRNA cut sites (Supplementary Fig. S4). Additionally, DNA sequencing of PCR fragments, amplified by primers surrounding predicted high-scoring off-target sites for each sgRNA, revealed no off-target mutations in PGP1 (Supplementary Table S3).

Functional Analysis of the Fluorescent Reporters in the PGP1

To test the function of PGP1 retinal reporter genes, we created retinal organoids from PGP1.hiPSCs, using a previously described protocol.[16] Only the VSX2:Cerulean reporter expressed at D20 of differentiation with fluorescence restricted to developing eye field domains (Supplementary Fig. S5). Manually isolated eye field domains (isolated between D20 and D24) formed spherical cups (Supplementary Fig. S6) with both Cerulean and eGFP expression by D55 (Figs. 3A, 3B). In the BRN3b reporter, the eGFP contained a GAP43 palmitoylation tag derived from the plasmid pCAG-mGFP to drive eGFP to the cell membrane,[26] which highlighted RGC axon bundles (Figs. 3B, 3D). At D55, sparse mCherry fluorescence, driven by *RCVRN* promoter, appeared sporadically throughout the organoids (Figs. 3C, 3D). A merged image of all three signals shows the restriction of fluorescent expression to distinct cells with little evidence of overlapping reporter expression (Fig. 3D, Supplementary Movie S1). Scanning parameters for Figure 3 and the Supplementary Movie S1 are supplied in Supplementary Table S9.

As the organoids matured, the ratio of cells expressing different fluorescent proteins changed. At D55, the majority of cells in the organoid expressed Cerulean, but as the organoids matured, the proportion of Cerulean expressing cells decreased (Figs. 3A, 3E, 3I). By D95, the eGFP-expressing axon bundles had disappeared, but punctate eGFP staining remained within the organoid and overall eGFP expression declined by D135 (Figs. 3F, 3J). This real-time decline in eGFP expression at later stages of organoid development correlates with the decline in the BRN3b mRNA levels (see Fig. 5E). Other laboratories have noted the challenge of long-term survival of retinal ganglion cells in three-dimensional retinal organoid culture.[27,28]

Figure 1. Creation of the neural retinal progenitor/retinal ganglion cell/photoreceptor (PGP1) reporter hiPSC line by CRISPR/Cas9 genome editing. (A) Schematic illustration of the generalized CRISPR/Cas9-mediated insertion strategy. CRISPR/Cas9 mediated the replacement of the endogenous STOP codon of *VSX2* (B), *BRN3b* (C), and *RCVRN* (D) loci with P2A:Cerulean, P2A:eGFP, and P2A:mCherry by homologous recombination in WT hiPSCs. Following nucleofection and triple antibiotic selection for puromycin (PURO), blasticidin (BLAST), and G418 (NEO), the resistant clones were screened by PCR with primer sets. (B) FW1/RV1 (forward primer [FW] located outside *VSX2* 5′HA and reverse primer [RV] located inside Cerulean) with the expected band size of 2.1 kb and FW2/RV2 (inside PURO to outside *VSX2* 3′HA) with the expected band size of 1.9 kb. (C) FW3/RV3 (outside *BRN3b* 5′HA to inside membrane tagged eGFP) with the expected band size of 1.7 kb and FW4/RV4 (inside BLAST to outside *BRN3b* 3′HA) with the expected band size of 1.5 kb. (D) FW5/RV5 (outside *RCVRN* 5′HA to inside mCherry) with the expected band size of 1.2 kb and FW6/RV6 (inside NEO to outside *RCVRN* 3′HA) with the expected band size of 1.5 kb. The WT hiPSC was used as control where no bands were seen. All the positive PCR bands were verified by sequencing. The original gels that were cropped for clarity in this figure (with white spaces between nonadjacent lanes) can be seen in their entirety in Supplementary Figure S9. Primer information listed in Supplementary Table S8.
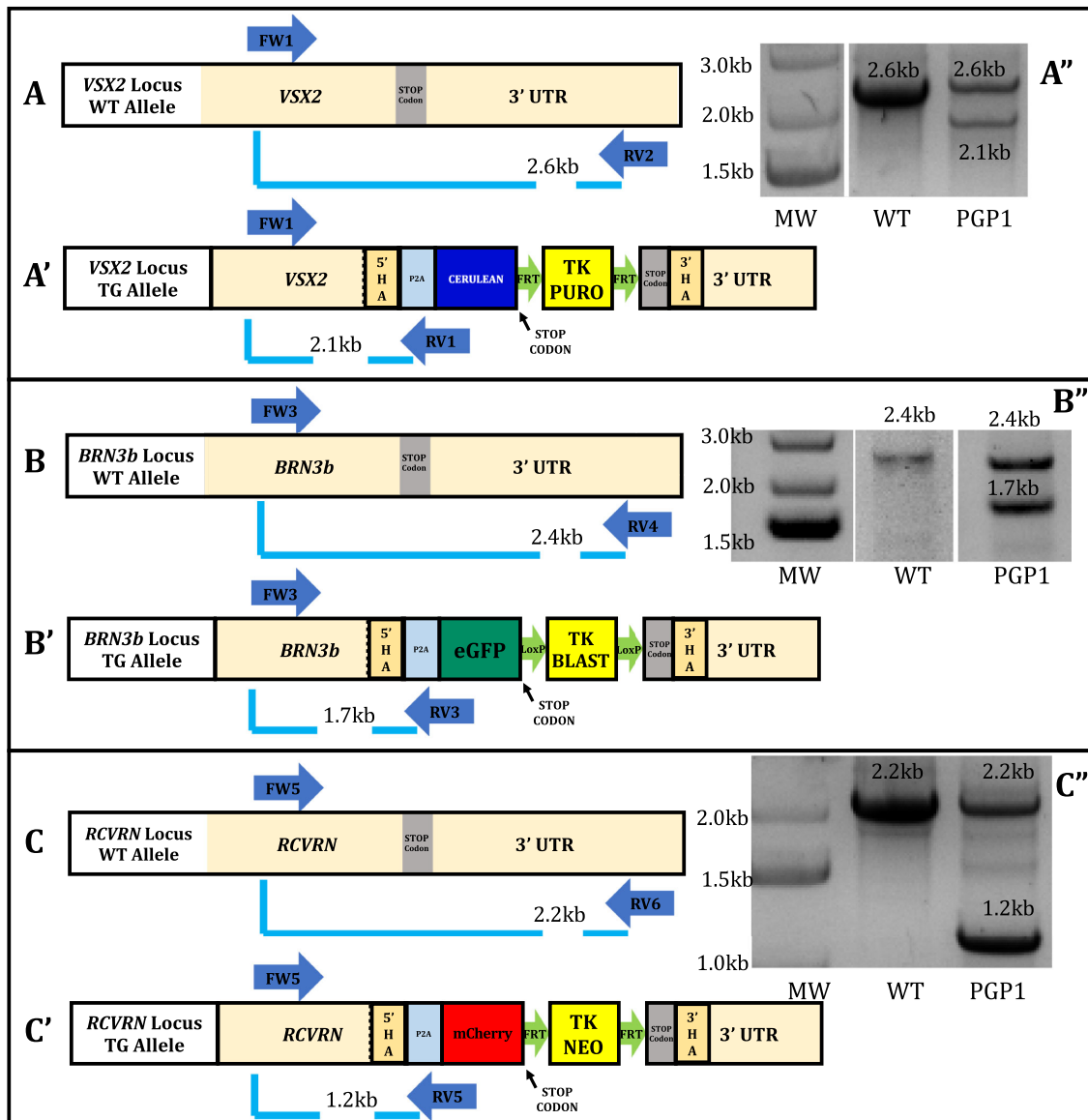
Figure 2. Determining the zygosity of the PGP1 line. In each case, a three-primer PCR strategy determined whether the PGP1 line was homozygous or heterozygous at the targeted loci. For the *VSX2* locus, primer FW1 is located outside the *VSX2* 5′HA, RV1 is located inside Cerulean, and RV2 is located outside the *VSX2* 3′HA. (A) The unedited *VSX2* allele (FW1/RV2) should generate a 2.6-kb band, (A′), whereas the edited *VSX2* allele (FW1/RV1) should generate a 2.1-kb band. (A′′) A gel image showed bands of 2.6 kb and 2.1 kb for the PGP1 line, whereas the WT hiPSC showed a 2.6-kb band indicating that PGP1 is heterozygous at the *VSX2* locus. For the *BRN3b* locus, FW3 is located outside the *BRN3b* 5′HA, RV3 is located inside the eGFP, and RV4 is located outside the *BRN3b* 3′HA. (B) The unedited *BRN3b* allele (FW3/RV4) should generate a 2.4-kb band, (B′) whereas the edited *BRN3b* allele (FW3/RV3) should generate a band of 1.7 kb. (B′′) A gel image showed bands of 2.4 kb and 1.7 kb for the PGP1 line, whereas the WT hiPSC showed only a 2.4-kb band, showing that PGP1 is heterozygous at the *BRN3b* locus. For the *RCVRN* locus, FW5 is located outside the *RCVRN* 5′HA, RV5 is located inside mCherry, and RV6 is located outside the *RCVRN* 3′HA. (C) The unedited *RCVRN* allele (FW5/RV6) should generate a 2.2-kb band, (C′) whereas the edited *RCVRN* allele (FW5/RV5) should generate a 1.2-kb band. (C′′) A gel image showed bands of 2.2 kb and 1.2 kb for the PGP1 line, whereas the WT hiPSC showed only a 2.2-kb band, indicating that PGP1 is heterozygous at the *RCVRN* locus. The original gels that were cropped for clarity in this figure (with white spaces between nonadjacent lanes) can be seen in their entirety in Supplementary Figure S10. Primer information listed in Supplementary Table S8.

The loss of eGFP-expressing retinal ganglion cell axon bundles in organoid culture may relate to a lack of synaptic contact to target brain regions.[29,30] Although only weak mCherry fluorescence appeared at D55, mCherry expression increased such that by D135, large areas of the organoid displayed mCherry fluorescence (Figs. 3C, 3G, 3K). Cerulean, eGFP, and mCherry signals did not appear to overlap either in the whole
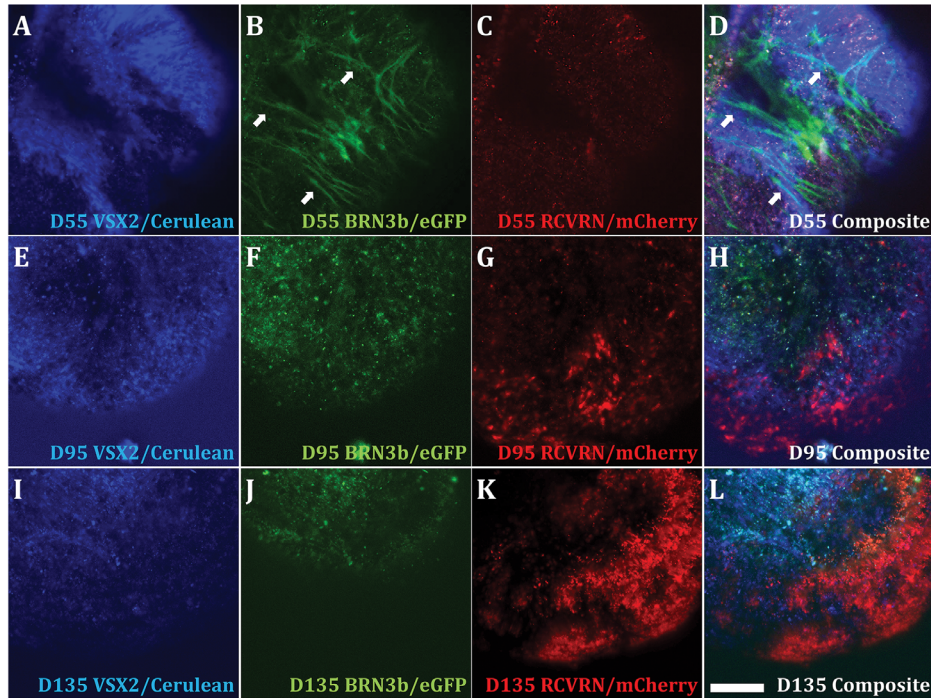
Figure 3. Functional analysis of the fluorescent reporters in the PGP1 line via retinal organoid formation. Single three-dimensional retinal organoids derived from the PGP1 hiPSC line were visualized by fluorescent microscopy at D55 (A, B, C, D), D95 (E, F, G, H), and D135 (I, J, K, L) of differentiation. Organoids were visualized with a 458-nm laser to excite Cerulean, driven by the *VSX2* promoter (A, E, I); a 488-nm laser to excite eGFP, driven by the *BRN3b* promoter (B, F, J); and both 543-nm and 633-nm lasers to excite mCherry, driven by the *RCVRN* promoter (C, G, K). Composite images represent the merger of all three fluorescent signals (D, H, L). The eGFP signal was targeted to the cell membrane by a GAP43 tag to allow for visualization of ganglion cell axon bundles (white arrows in B, D). As organoids matured from D55 to D135, the number of cells expressing mCherry dramatically increased (compare C and K), and the eGFP$^+$ cells populated the interior of the organoid (J) while the mCherry$^+$ cells occupied the organoid periphery (K). Magnification bar: 100 μm. Scanning parameters are in Supplementary Table S9.

mounts or in the optical section Z-stack (Supplementary Movie S1).

To confirm that the observed fluorescent proteins identified the targeted cell types, we sorted organoid cells based on fluorescent protein expression. At D55, the organoids contained large numbers of Cerulean and eGFP$^+$ cells but relatively fewer mCherry$^+$ cells. By D135, the organoids contained abundant mCherry$^+$ cells. Considering this, we performed FACS on single cell suspensions to collect Cerulean$^+$ and eGFP$^+$ (Figs. 4A, 4D) cells from D55 and mCherry$^+$ (Fig. 4G) cells from D135 organoids. At D55, Cerulean$^+$ and eGFP$^+$ cells comprised approximately 11.3% and 4.9% of the single cells from disaggregated organoids, respectively. At D135, approximately 53% of organoid cells were mCherry$^+$. We also sorted organoids from WT hiPSCs using the same gates used for the PGP1-derived organoids and found no cells within the Cerulean (Fig. 4J), eGFP (Fig. 4K), or mCherry (Fig. 4L) gates. Because FACS can only analyze single cells, it remains possible that certain organoid cell types exhibit increased resistance to single cell dissociation that could bias our quantitative analysis. However, this bias should not influence comparative analysis between expressing and nonexpressing cells for any single fluorescent protein.

We performed RT-qPCR and immunofluorescence to determine if fluorescent reporter expression correlated with the expression of the targeted gene in sorted samples. The transcript analysis revealed that the sorted Cerulean$^+$ population (Fig. 4A) expressed significantly more Cerulean mRNA than the Cerulean$^-$ population (Fig. 4B). Likewise, the Cerulean$^+$ population expressed approximately three times more *VSX2* mRNA than the Cerulean$^-$ population (Fig. 4C). The eGFP$^+$ sorted population (Fig. 4D) expressed 22-fold more eGFP mRNA and 9.1-fold more *BRN3b* mRNA than the eGFP$^-$ population (Figs. 4E, 4F). On D135, the mCherry$^+$ (Fig. 4G) population expressed approximately 4.9 times more mCherry mRNA and 1.9 times more *RCVRN* mRNA than the mCherry$^-$ population (Figs. 4H, 4I). For *VSX2* and *BRN3b*, the majority of expressing cells appeared in the Cerulean$^+$ and eGFP$^+$ populations, respectively. The
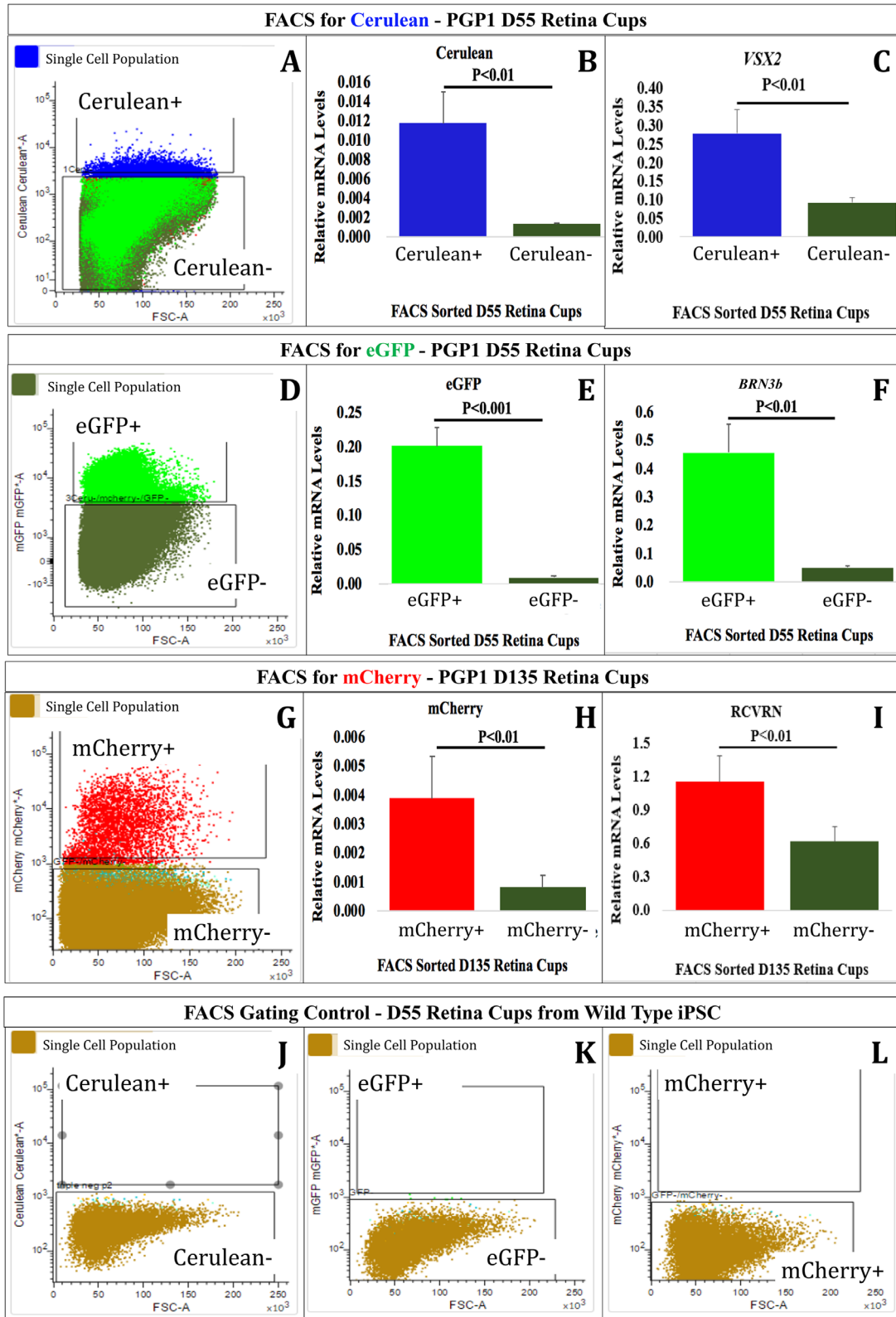
Figure 4. Confirmation of PGP1-derived retinal organoids corresponded to the appropriately targeted cell types. At D55 (A–F, J–L) and D135 (G–I), the retinal organoids were dissociated into single cells and used for FACS analysis. At D55, (A) the Cerulean⁺ population was sorted from the Cerulean⁻ population. RT-qPCR analysis revealed that the Cerulean⁺ cells expressed significantly more Cerulean mRNA (B) and *VSX2* mRNA (C) than the Cerulean⁻ cells. Also, at D55, (D) the eGFP⁺ population was sorted from the eGFP⁻ population. RT-qPCR analysis demonstrated that the eGFP⁺ cells expressed significantly more eGFP mRNA (E) and *BRN3b* mRNA (F) than the eGFP⁻ cells. At

appearance of relatively more *RCVRN* transcripts in the mCherry⁻ population than *BRN3b* transcripts in the eGFP⁻ or *VSX2* transcripts in the Cerulean⁻ populations suggests that not all RCVRN-expressing cells express mCherry. Double immunohistochemical analysis of D55 organoids revealed colabeling of BRN3 and GFP (Supplementary Figs. S7A–C), whereas D163 organoids showed colabeling of VSX2 and GFP (Supplementary Figs. S7D–F). Note that in both of the above cases, our antibody cannot distinguish GFP from Cerulean. Although antibodies for RCVRN colabel cells that express mCherry in D163 organoids (Supplementary Figs. S7G–I), the organoids exhibited some RCVRN-expressing cells that failed to express mCherry. However, this same analysis showed that all mCherry⁺ cells coexpressed RCVRN. The RCVRN⁺/mCherry⁻ proportion of cells exhibited organoid-to-organoid variability (Supplementary Fig. S8). All of the positive and negative sorted populations for each fluorescent protein were tested by RT-qPCR in triplicate (Figs. 4B, 4C, 4E, 4F, 4H, 4I). These data demonstrate that the reporters faithfully reveal the target gene-expressing cells. Although we did not conduct FACS analyses on organoids formed by any of the other triple targeted hiPSC lines, we did confirm that clones 56 and 101, in addition to PGP1 (122), formed organoids expressing all three fluorescent proteins.

PGP1-Derived Retinal Organoids Contain All Major Retinal Cell Types

A comparison of transcripts expressed by PGP1 hiPSCs at D0 of differentiation with those expressed by PGP1-derived retinal organoids at D55 revealed a decrease in pluripotency-related genes and an increase in retinal differentiation-related genes. Pluripotency transcripts for *OCT4* (*POU5F1*) and *NANOG* expressed abundantly at D0 (Fig. 5A). In contrast, the NRP transcripts (*PAX6*, *SIX3*, and *LHX2*) (Fig. 5B) and retinal pigment epithelium (*MITF* and *BEST1*) transcripts (Fig. 5C) increased significantly during early retinal organoid differentiation at D55. In addition, a sequential expression of NRPs (*VSX2*) and RGCs (*BRN3b*) revealed a decline, whereas the level of PRs' transcript (*RCVRN*) increased signifi-

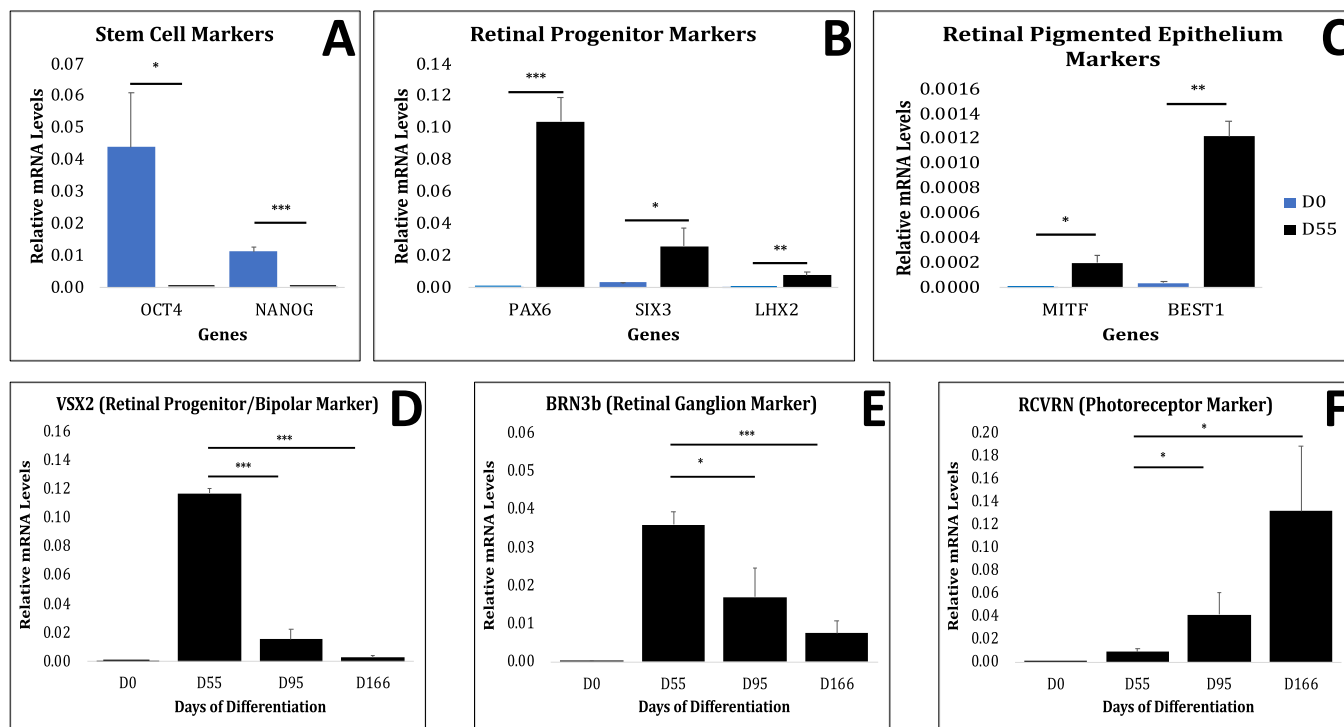cantly from D55 to D166 of differentiation (Figs. 5D, 5E, 5F).

PGP1-derived organoids contained cells of all major retinal cell types. At D55, organoids expressed the eye field precursor protein RX (Fig. 6A); NRP markers PAX6, SIX3, and VSX2 (Figs. 6B–D); and the proliferation marker MCM2 (Fig. 6E) throughout the D55 organoid tissue. In contrast, the expression of BRN3b (marking RGCs) localized interiorly (outlined in Fig. 6F), as did AP2-*α* (amacrine cell marker) by D70 (outlined in Fig. 6G). Although RCVRN (PR marker) initially appeared throughout the organoid, by D70, RCVRN appeared near the organoid periphery (Fig. 6H). At D95, PROX1 (horizontal cell marker) was located below the putative outer nuclear layer (Fig. 6I). CRALBP, a marker of the late-differentiating Müller glia cells, appeared through the full thickness of the retinal organoids at D163 (Fig. 6J). Although VSX2 expression initially characterized proliferating (MCM2 positive) NRP cells, VSX2 appeared later in nonproliferating (MCM2 negative) bipolar cells. These VSX2 positive/MCM2 negative bipolar cells increased in abundance by D163 (Figs. 6K, 6L).

Discussion

We created an hiPSC line (PGP1) for real-time analysis of NR differentiation with multiple retinal cell type–specific reporters via CRISPR/Cas9 genome editing. Furthermore, we functionally characterized PGP1 both by fluorescent protein expression and by differentiation into all major retinal cell types during retinal organoid formation. Although previous reports described single retinal cell type–specific reporters, to our knowledge, PGP1 represents the first triple targeted retinal reporter hiPSC line.[5–7] The ability of the PGP1 to facilitate visual observation of retinal differentiation, without compromising retinal organoid formation typical of WT hiPSCs,[25] makes this clone particularly useful for several applications.

PGP1 provides a powerful tool for real-time retinal disease modeling. For example, hiPSC-derived organoids from patients with mutations leading to retinitis pigmentosa and Leber congenital amaurosis have provided important insights about the

Figure 5. Retinal development is recapitulated in the differentiating PGP1 hiPSC-derived retinal organoids. (A–C) Undifferentiated PGP1 hiPSCs day 0 (D0, blue) and differentiated PGP1 retinal organoids at day 55 (D55, black) were used to measure mRNA levels of various markers via RT-qPCR normalized to *GAPDH*. (A) Expression of stem cell markers OCT4, NANOG; (B) NRP markers PAX6, SIX3, LHX2; (C) Retinal pigment epithelium (RPE) markers *MITF*, *BEST1*. (D–F) PGP1 hiPSCs at D0 and hiPSCs retinal organoids at D55, D95, and D166 of differentiation were used to measure mRNA levels via RT-qPCR normalized to *GAPDH*. (D) NRP and bipolar marker *VSX2*, (E) RGC marker BRN3*b*, and (F) PR marker RCVRN. As organoid differentiation progressed from D0 to D55, stem cell markers significantly decreased and markers of retina and RPE differentiation significantly increased. Compared to D55, the PR marker *RCVRN* progressively increased in its mRNA expression, whereas the NRP marker *VSX2* and the RGC marker *BRN3b* gradually decreased in the older retinal organoids. Error bars represent standard error of the mean (SE), paired *t* test. *$P < 0.05$. **$P < 0.005$. ***$P < 0.0005$. Primer information is listed in Supplementary Table S5.

pathobiology of these diseases.[31–34] Likewise, RGCs with specific mutations, differentiated from patient-derived hiPSCs, have provided models for optic atrophy and glaucoma.[35,36] The relative ease of creating specific mutations with CRISPR/Cas9 genome editing should make it possible to take advantage of the cell type–specific reporters in PGP1 when modeling genetic retinal diseases.[32]

PGP1-derived retinal organoids will provide a platform to screen drugs to treat retinal damage. A number of different physical or chemical insults can result in PR injury, making the search for compounds that can prevent or minimize such damage very important. Retinal organoids made from mouse induced pluripotent stem cells, with a Nrl-eGFP reporter to label rod PRs, facilitated the testing of compounds to protect PRs from 4-hydroxytamoxifen-induced degeneration.[37] Additionally, the recently reported three-dimensional automated reporter quantification technology[38] would make screening drugs that affect retinal development and/or survival straightforward

in PGP1-derived organoids. Therefore, the use of PGP1 hiPSCs for such a purpose would have the added advantage of simultaneous real-time monitoring of NRPs and PRs without having to fix the organoid and terminate the experiment. In fact, the loss of fluorescence in the PGP1-derived organoids postfixation (Supplementary Fig. S1) presents a small limitation of using this line for terminal analysis. However, immunohistochemistry can reveal mCherry and GFP/Cerulean expression in fixed organoid tissue (Supplementary Fig. S7). In fact, we consider the loss of reporter protein fluorescence postfixation as an advantage because it removes a potentially interfering signal from subsequent immunohistochemical analysis with fluorescent secondary antibodies.

PGP1 hiPSCs will facilitate protocol optimization to achieve the differentiation and/or survival of specific retinal cell types. For example, improved mature PR yields and laminar stratification resulted from the use of stirred-tank bioreactors, due to increased cell proliferation and decreased apoptosis.[38]
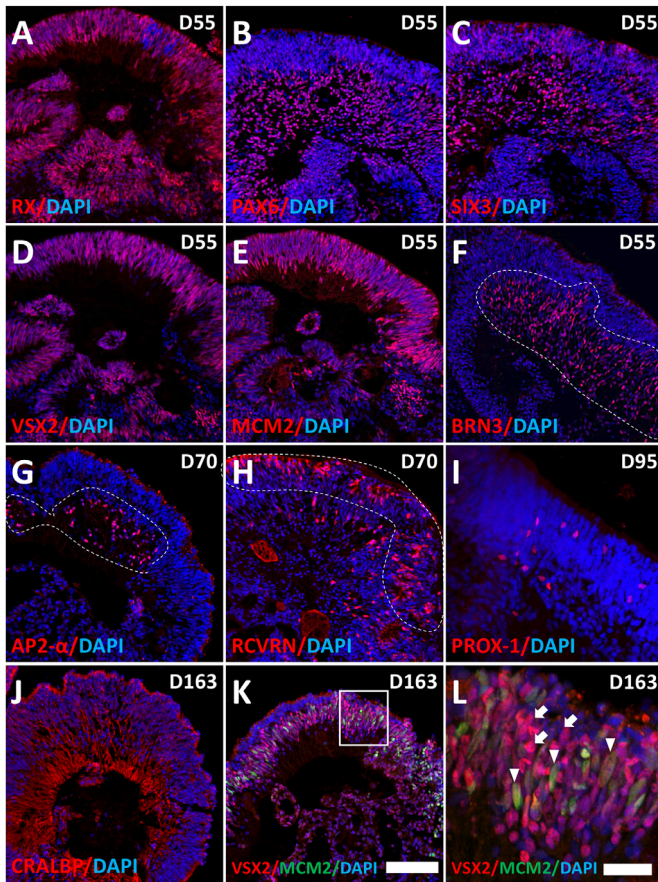
Figure 6. Retinal organoids differentiated from PGP1 line contain all major retinal cell types. At D55 of retinal organoid differentiation, the organoids were analyzed by immunohistochemistry using antibodies for the eye-field precursor marker RX (A), neuronal markers PAX6 (B) and SIX3 (C), the NRP marker VSX2 (D), the proliferation marker MCM2 (E), and the RGC marker BRN3 (F). At D70 of the retinal organoid differentiation, the organoids contained the amacrine cell marker AP2-α (G) and the photoreceptor marker RCVRN (H). The organoids contained the horizontal cell marker PROX-1 (I) at D95 and the Müller glia cell marker CRALBP (J) at D163. Also, at D163, the organoids contained the bipolar cell marker VSX2$^+$/MCM2$^-$ (K, L). (L) An enlarged view of the boxed area in (K) where VSX2$^+$/MCM2$^+$ (white arrowheads) cells represent NRPs and the VSX2$^+$/MCM2$^-$ (white arrows) cells represent bipolar cells at D163. Dotted lines emphasize that the major expression domains of Brn3b (F), AP2α (G), and Prox1 (I) appear on the interior of the organoids, whereas RCVRN (H) is predominantly on the organoid periphery. Magnification bar: 100 μm (A–K); 25 μm (L). Antibodies used for immunohistochemistry listed in Supplementary Table S6.

This study used immunohistochemical and FACS-mediated immunopurification of organoid-derived cell types. PGP1-derived organoids would permit similar protocol optimization for multiple cell types in real time without relying on antibody labels. Additionally, the decline of ganglion axon bundles in late-stage organoids observed in our line and other published observations[28–30] presents a challenge for culturing RGCs with our current organoid protocol. The PGP1-dervied organoids would permit protocol optimization for long-term survival of RGCs and axon bundles in late-stage organoids. Therefore, the ability to continuously monitor RGCs and PRs should improve optimization for long-term survival of these cell types.

PGP1 hiPSCs could provide an effective strategy for improved purification of specific cell types. In direct differentiation protocols to achieve particular retinal cell types from hiPSCs, purifying fully differentiated, mature cell types remains an issue.[39] The purification of specific retinal neurons can often facilitate downstream analysis or transplantation studies. Recombinant AAV (Adeno-associated Virus) viruses containing a GFP reporter driven by an L/M cone-specific promoter led to the successful FACS isolation of cone PRs from both human fetal retina and from hiPSC-derived retinal organoids.[40] A similar strategy used recombinant lentivirus to achieve GFP expression from the PR-specific (IRBP) promoter to achieve FACS purification of hiPSC-derived PR cells prior to transplantation into immunocompromised mice.[41] Although both of these reports relied on virus-mediated reporter gene expression, others have adopted the use of endogenous reporters. For example, hiPSCs engineered with a P2A peptide-mCherry reporter into the *BRN3b* locus facilitated the purification of viable RGCs from retinal organoids by FACS.[5] These examples all attest to the potential of the PGP1 line for purification of specific retinal cell types. However, the unique feature of the PGP1 line lies in its potential for simultaneously purifying NRPs, RGCs, PRs, and bipolar cells.

hiPSC lines with multiple cell type–specific reporters could serve as a powerful tool for proof-of-concept studies and for tracking retinal-specific cell fates posttransplantation in animal models. For example, transplanting human NRPs into a mouse glaucoma model increased host RGC survival.[42] In the future, PGP1-derived cells will make it possible to evaluate the fate of transplanted cells in animal models in vivo. In these transplants, PGP1-derived NRPs, and later bipolar cells, would exhibit blue fluorescence, whereas RGCs or PRs derived from the transplant would exhibit green or red fluorescence, respectively. In another study, transplantation of GFP-labeled human PRs into a rat model of retinitis pigmentosa demonstrated restoration of the host rod function.[43] Although these authors reported integration of GFP-positive PRs into the outer nuclear layer, the recent realization of cytoplasmic transfer from donor to host cells in PR transplantation[44,45] necessitates further confirmation of donor cell integration. Transplantation of PGP1-derived NRPs into an animal model of retinal degeneration would only result in GFP$^+$

ganglion cells or mCherry$^+$ PRs if these NRPs differentiated into these cell types in situ. These experiments could provide more definitive proof of donor cell integration and could also serve as an indicator of both cell survival and cell fate of the transplanted NRPs.

In summary, we demonstrate a CRISPR/Cas9 strategy to target the expression of multiple fluorescent reporter genes into endogenous loci in hiPSCs. In doing so, we created a triple transgenic hiPSC line (PGP1) and tested the function of this line by directed differentiation into three-dimensional retinal organoids. Organoids produced from the PGP1 line expressed Cerulean in NRPs and bipolar cells, membrane-targeted eGFP in RGCs, and mCherry in PRs. In addition, PGP1-derived retinal organoids contained all major retinal cell types. The usefulness of this strategy extends to virtually any cell type–specific gene, limited only by the number of different fluorescent reporters available for simultaneous analysis. The PGP1 line and subsequent hiPSC lines developed using this approach hold great promise for studying retinal development, disease modeling, drug screening, and preclinical transplantation studies.

Acknowledgments

PTL designed and conducted all CRISPR/Cas9 targeting and screening of hiPSC lines, performed all immunohistochemistry and confocal microscopy, and designed and conducted all RT-qPCR analysis and FACS sorting. CG conducted all retinal organoid cultures and assisted with immunohistochemistry. KDR-T participated in experimental design and reviewed all of the data for the manuscript. MLR supervised all experiments, participated in all aspects of experimental design, and reviewed all the data. PTL and MLR wrote the manuscript. All authors reviewed and edited the manuscript.

References

1. Sowden JC. ESC-derived retinal pigmented epithelial cell transplants in patients: so far, so good. *Cell Stem Cell*. 2014;15:537–538.

2. Veleri S, Lazar CH, Chang B, Sieving PA, Banin E, Swaroop A. Biology and therapy of inherited retinal degenerative disease: insights from mouse models. *Dis Model Mech*. 2015;8:109–129.

3. Llonch S, Carido M, Ader M. Organoid technology for retinal repair. *Dev Biol*. 2018;433:132–143.

4. DiStefano T, Chen HY, Panebianco C, et al. Accelerated and improved differentiation of retinal organoids from pluripotent stem cells in rotating-wall vessel bioreactors. *Stem Cell Rep*. 2018;10:300–313.

5. Sluch VM, Davis C-HO, Ranganathan V, et al. Differentiation of human ESCs to retinal ganglion cells using a CRISPR engineered reporter cell line. *Sci Rep*. 2015;5:16595.

6. Sluch VM, Chamling X, Liu MM, et al. Enhanced stem cell differentiation and immunopurification of genome engineered human retinal ganglion cells. *Stem Cells Transl Med*. 2017;6:1972–1986.

7. Phillips MJ, Joseph Phillips M, Capowski EE, et al. Generation of a rod-specific NRL reporter line in human pluripotent stem cells. *Sci Rep*. 2018;8.

8. Shirai H, Mandai M, Matsushita K, et al. Transplantation of human embryonic stem cell-derived retinal tissue in two primate models of retinal degeneration. *Proc Natl Acad Sci USA*. 2016;113:E81–E90.

9. Jin Z-B, Okamoto S, Osakada F, et al. Modeling retinal degeneration using patient-specific induced pluripotent stem cells. *PLoS One*. 2011;6:e17084.

10. Zou C, Levine EM. Vsx2 controls eye organogenesis and retinal progenitor identity via homeodomain and non-homeodomain residues required for high affinity DNA binding. *PLoS Genet*. 2012;8:e1002924.

11. Phillips MJ, Perez ET, Martin JM, et al. Modeling human retinal development with patient-specific

induced pluripotent stem cells reveals multiple roles for visual system homeobox 2. *Stem Cells*. 2014;32:1480–1492.

12. Badea TC, Cahill H, Ecker J, Hattar S, Nathans J. Distinct roles of transcription factors brn3a and brn3b in controlling the development, morphology, and function of retinal ganglion cells. *Neuron*. 2009;61:852–864.

13. Polans AS, Witkowska D, Haley TL, Amundson D, Baizer L, Adamus G. Recoverin, a photoreceptor-specific calcium-binding protein, is expressed by the tumor of a patient with cancer-associated retinopathy. *Proc Natl Acad Sci USA*. 1995;92:9176–9180.

14. Cao D, Barrionuevo PA. Estimating photoreceptor excitations from spectral outputs of a personal light exposure measurement device. *Chronobiol Int*. 2015;32:270–280.

15. Wang Y, Wang F, Wang R, Zhao P, Xia Q. 2A self-cleaving peptide-based multi-gene expression system in the silkworm Bombyx mori. *Sci Rep*. 2015;5:16273.

16. Ran FA, Ann Ran F, Hsu PD, et al. Genome engineering using the CRISPR-Cas9 system. *Nat Protoc*. 2013;8:2281–2308.

17. Vouillot L, Thélie A, Pollet N. Comparison of T7E1 and surveyor mismatch cleavage assays to detect mutations triggered by engineered nucleases. *G3 (Bethesda)*. 2015;5:407–415.

18. Liu P, Jenkins NA, Copeland NG. A highly efficient recombineering-based method for generating conditional knockout mutations. *Genome Res*. 2003;13:476–484.

19. Megason SG. In toto imaging of embryogenesis with confocal time-lapse microscopy. *Methods Mol Biol*. 2009;546:317–332.

20. Matsuda T, Cepko CL. Controlled expression of transgenes introduced by in vivo electroporation. *Proc Natl Acad Sci USA*. 2007;104:1027–1032.

21. Provost E, Rhee J, Leach SD. Viral 2A peptides allow expression of multiple proteins from a single ORF in transgenic zebrafish embryos. *Genesis*. 2007;45:625–629.

22. Burridge PW, Thompson S, Millrod MA, et al. A universal system for highly efficient cardiac differentiation of human induced pluripotent stem cells that eliminates interline variability. *PLoS One*. 2011;6:e18293.

23. Chen G, Gulbranson DR, Hou Z, et al. Chemically defined conditions for human iPSC derivation and culture. *Nat Methods*. 2011;8:424–429.

24. Benchling. Better tools, faster research. Available at: https://benchling.com/crispr. Accessed February 8, 2018.

25. Zhong X, Gutierrez C, Xue T, et al. Generation of three-dimensional retinal tissue with functional photoreceptors from human iPSCs. *Nat Commun*. 2014;5:4047.

26. Gauthier-Kemper A, Igaev M, Sündermann F, et al. Interplay between phosphorylation and palmitoylation mediates plasma membrane targeting and sorting of GAP43. *Mol Biol Cell*. 2014;25:3284–3299.

27. DiStefano T, Chen HY, Panebianco C, et al. Accelerated and improved differentiation of retinal organoids from pluripotent stem cells in rotating-wall vessel bioreactors. *Stem Cell Reports*. 2018;10:300–313.

28. Tanaka T, Yokoi T, Tamalu F, Watanabe S-I, Nishina S, Azuma N. Generation of retinal ganglion cells with functional axons from human induced pluripotent stem cells. *Sci Rep*. 2015;5:8344.

29. Isenmann S, Kretz A, Cellerino A. Molecular determinants of retinal ganglion cell development, survival, and regeneration. *Prog Retin Eye Res*. 2003;22:483–543.

30. Lom B, Cohen-Cory S. Brain-derived neurotrophic factor differentially regulates retinal ganglion cell dendritic and axonal arborization in vivo. *J Neurosci*. 1999;19:9928–9938.

31. Parfitt DA, Lane A, Ramsden CM, et al. Identification and correction of mechanisms underlying inherited blindness in human iPSC-derived optic cups. *Cell Stem Cell*. 2016;18:769–781.

32. Schwarz N, Lane A, Jovanovic K, et al. Arl3 and RP2 regulate the trafficking of ciliary tip kinesins. *Hum Mol Genet*. 2017;26:3451.

33. Tucker BA, Mullins RF, Streb LM, et al. Patient-specific iPSC-derived photoreceptor precursor cells as a means to investigate retinitis pigmentosa. *Elife*. 2013;2:e00824.

34. Megaw R, Abu-Arafeh H, Jungnickel M, et al. Gelsolin dysfunction causes photoreceptor loss in induced pluripotent cell and animal retinitis pigmentosa models. *Nat Commun*. 2017;8: 271.

35. Chen J, Riazifar H, Guan M-X, Huang T. Modeling autosomal dominant optic atrophy using induced pluripotent stem cells and identifying potential therapeutic targets. *Stem Cell Res Ther*. 2016;7:2.

36. Teotia P, Van Hook MJ, Wichman CS, Allingham RR, Hauser MA, Ahmad I. Modeling glaucoma: retinal ganglion cells generated from induced pluripotent stem cells of patients with SIX6 risk allele show developmental abnormalities. *Stem Cells*. 2017;35:2239–2252.

37. Ito S-I, Onishi A, Takahashi M. Chemically-induced photoreceptor degeneration and protection in mouse iPSC-derived three-dimensional retinal organoids. *Stem Cell Res*. 2017;24:94–101.

38. Ovando-Roche P, West EL, Branch MJ, et al. Use of bioreactors for culturing human retinal organoids improves photoreceptor yields. *Stem Cell Res Ther*. 2018;9:156.

39. Tano K, Yasuda S, Kuroda T, Saito H, Umezawa A, Sato Y. A novel in vitro method for detecting undifferentiated human pluripotent stem cells as impurities in cell therapy products using a highly efficient culture system. *PLoS One*. 2014;9:e110496.

40. Welby E, Lakowski J, Di Foggia V, et al. Isolation And Comparative Transcriptome Analysis Of Human Fetal and iPSC-derived cone photoreceptor cells. *Stem Cell Reports*. 2017;9:1898–1915.

41. Lamba DA, McUsic A, Hirata RK, Wang P-R, Russell D, Reh TA. Generation, purification and transplantation of photoreceptors derived from human induced pluripotent stem cells. *PLoS One*. 2010;5:e8763.

42. Ma J, Guo C, Guo C, et al. Transplantation of human neural progenitor cells expressing IGF-1 enhances retinal ganglion cell survival. *PLoS One*. 2015;10:e0125695.

43. Jayaram H, Jones MF, Eastlake K, et al. Transplantation of photoreceptors derived from human Muller glia restore rod function in the P23H rat. *Stem Cells Transl Med*. 2014;3:323–333.

44. Nickerson PEB, Ortin-Martinez A, Wallace VA. Material exchange in photoreceptor transplantation: updating our understanding of donor/host communication and the future of cell engraftment science. *Front Neural Circuits*. 2018;12:17.

45. Ortin-Martinez A, et al. A reinterpretation of cell transplantation: GFP transfer from donor to host photoreceptors. *Stem Cells*. 2017;35:932–939.

Supplementary Material

Supplementary Movie S1. Z-stacked, three-dimensional confocal image of a portion of a PGP1-derived retinal organoid demonstrating the expression of Cerulean, eGFP, and mCherry at Day 55 of differentiation.